

New Bag of Deep Visual Words based Features to Classify Chest X-ray Images for COVID-19 diagnosis

Chiranjibi Sitaula ✉ · Sunil Aryal

Received: DD Month YEAR / Accepted: DD Month YEAR

Abstract Purpose: Because the infection by Severe Acute Respiratory Syndrome Coronavirus 2 (COVID-19) causes the pneumonia-like effect in the lung, the examination of Chest X-Rays (CXR) can help diagnose the disease. For automatic analysis of images, they are represented in machines by a set of semantic features. Deep Learning (DL) models are widely used to extract features from images. General deep features extracted from intermediate layers may not be appropriate to represent CXR images as they have a few semantic regions. Though the Bag of Visual Words (BoVW)-based features are shown to be more appropriate for different types of images, existing BoVW features may not capture enough information to differentiate COVID-19 infection from other pneumonia-related infections. **Methods:** In this paper, we propose a new BoVW method over deep features, called Bag of Deep Visual Words (BoDVW), by removing the feature map normalization step and adding the deep features normalization step on the raw feature maps. This helps to preserve the semantics of each feature map that may have important clues to differentiate COVID-19 from pneumonia. **Results:** We evaluate the effectiveness of our proposed BoDVW features in CXR image classification using Support Vector Machine (SVM) to diagnose COVID-19. Our results on four publicly available COVID-19 CXR image datasets reveal that our features produce stable and prominent classification accuracy, particularly differentiating COVID-19 infection from other pneumonia. **Conclusion:** Our method could

be a very useful tool for the quick diagnosis of COVID-19 patients on a large scale.

Keywords Bag of Visual Words (BoVW) · Bag of Deep Visual Words (BoDVW) · Chest X-Ray · COVID-19 · Deep Features · SARS-CoV-2

1 Introduction

The disease caused by Severe Acute Respiratory Syndrome Coronavirus 2 (SARS-CoV-2) [24, 29, 44], commonly known as COVID-19, was originated in Wuhan city of China in late 2019 [46]. It is believed to be originated from bats [25, 35]. The virus has been transmitting from human to human all around the world [16, 11, 3]. It has spread over 200 countries in the world at present and become a pandemic that has killed 2,184,120 people¹ and 909 people in Australia alone², so far. While analyzing the effect of the SARS-CoV-2 virus in the human body, it has been known that it causes the pneumonia-like effect in the lungs. Thus, the study of chest x-ray images could be an alternative to a swab test for early quick diagnosis of the COVID-19. An automated chest x-ray (CXR) image analysis tool can be very useful to health practitioners for mass screening of people quickly.

For automatic analysis of images using algorithms, they are represented in machines by a set of semantic features. Large artificial neural networks, also known

¹ <https://www.worldometers.info/coronavirus/> (accessed date: 28/01/2021)

² <https://www.health.gov.au/news/health-alerts/novel-coronavirus-2019-ncov-health-alert/coronavirus-covid-19-current-situation-and-case-numbers>. (accessed date: 28/01/2021)

as Deep Learning (DL) models, are widely used to extract features from images and shown to work well in various types of images [51, 47, 49, 50, 13, 34]. A few research studies have used DL models to analyze CXR images for coronavirus diagnosis, too. For instance, two recent works [30, 34] include the fine-tuning approach of transfer-learning on pre-trained DL models such as AlexNet [22], ResNet-18 [14], GoogleNet [53], etc. These methods normally require a massive amount of data to learn the separable features in addition to extensive hyper-parameter tuning tasks. However, most of the biomedical images (e.g., COVID-19 CXR images) are normally limited because of privacy issues. Thus, working on a limited amount of data is always a challenging problem in deep learning (DL) models. Similarly, unlike other types of images, existing feature extraction methods such as GAP (Global Average Pooling) features achieved from pre-trained models may not provide accurate representation for CXR images because of their sparsity (i.e., having fewer semantic regions in them). Also, CXR images of lungs infected by COVID-19 and other pneumonia look similar (i.e., there is a high degree of inter-class similarities). There might be subtle differences at very basic level, which, in our understanding, may be captured using the Bag of Words approach over deep features.

Bag of Visual Words (BoVW)-based features are shown to be more appropriate in images with the characteristics discussed above (sparsity and high inter-class similarity). They consider visual patterns/clues (known as visual words) in each image in the collection, thereby capturing sparse interesting regions in the image, which are useful in dealing with the inter-class similarity problem to some degree. BoVW-based feature extraction approach is popular not only in traditional computer vision-based methods such as Scale Invariant Features Transform (SIFT) [31] but also in DL-based methods due to its ability to capture semantic information extracted from the feature map of pre-trained DL models. The Bag of Deep Visual Words (BoDVW) features designed for one domain may not work well for another domain due to the varying nature of the images. For example, the Bag of Deep Convolutional Features (DCF-BoVW) [56] designed for satellite images may not work exactly for biomedical images such as CXR images. This is because of the fact that satellite image contains numerous semantic regions scattered in the image (dense) and thus, DCF-BoVW could capture enough semantic regions of such images. However, the CXR images contain fewer semantic regions (sparse), which may not be captured accurately by DCF-BoVW.

In this paper, we propose a new BoDVW-based feature extraction method to represent CXR images. Our

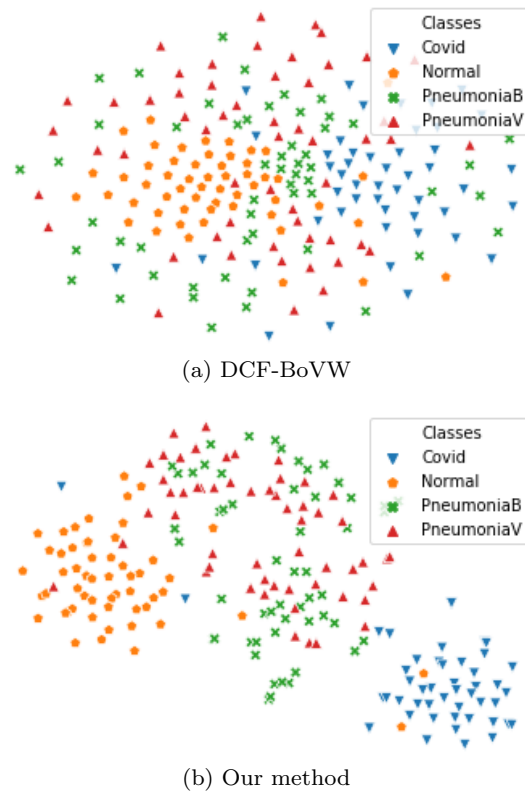


Fig. 1 Scatter plot of two dimensional projection of features produced by DCF-BoVW and our proposed method based on t-SNE visualization on chest x-ray images of Dataset 4 [8, 20].

method eliminates some of the intermediate steps present in DCF-BoVW [56] and adds new steps because of the nature of CXR images. For this, we adopt the following steps. First, we extract the raw feature map from the mid-level (4th pooling layer) of the VGG16 pre-trained DL model [45] for each input image. We prefer the 4th pooling layer in our work, which has been chosen by empirical study and suggestion from recent work by Sitaula et al. [48]. Next, we perform L2-normalization of each deep feature vector over the depth of the feature map. Using the training set, we design a codebook/dictionary over such deep features extracted from all the training images. Next, based on the codebook, we achieve our proposed features using a bag of visual words method for each input image. Last, such features based on the bag of visual words method is normalized by L2-norm, which acts as the final representation of the input image. Because our final features are based on patterns extracted from mid-level features from training images, they capture the more discriminating clues of sparse CXR images. The comparison of two-dimensional projections of features produced by DCF-BoVW and our proposed method on the COVID-19 image dataset [8] based on the t-SNE visualization

[33] is shown in Fig. 1. It reveals that our features impart the higher separability among different classes.

The main **contributions** in our work are listed below:

- (a) Propose to use the improved version of a bag of visual words method over deep features to work for the covid-19 CXR image representation.
- (b) Analyze the classification performance of our method across deep features extracted from five different pooling layers of the VGG16 model. Due to higher discriminability of deep features extracted from mid-level VGG16 model (see details in Sec. 4.4 and Sitaula et al. [48]), we leverage fourth pooling layer (p_4) for feature extraction in our work. To design a codebook from deep features in our work, we use unsupervised clustering with the simple k -means algorithm.
- (c) Evaluate our method on four datasets against the state-of-the-art methods based on pre-trained DL models in the covid-19 CXR classification task using the Support Vector Machine (SVM) classifier. The results show that our method produces stable and state-of-the-art classification performance.

The remainder of the paper is organized as follows. In Sec. 2, we review some of the recent related works on CXR image representation and classification. Similarly, we discuss our proposed method in Sec. 3 in a step-wise manner. Furthermore, Sec. 4 details the experimental setup, performance comparison, and ablation study associated with it. Finally, Sec. 5 concludes our paper with potential directions for future research.

2 Related works

Deep Learning (DL) has been a breakthrough in image processing producing significant performance improvement in tasks such as classification, object detection, etc. A DL model is a large Artificial Neural Network (ANN), which has been designed based on the working paradigm of brain. If we design our DL model from scratch and train it, it is called a user-defined DL model. Similarly, if we use existing deep learning architectures pre-trained on large datasets, such as ImageNet [10] or Places [57], they are called pre-trained DL models. The features extracted from intermediate layers of DL models, either user-defined or pre-trained, provide rich semantic features to represent images that result in significantly better task-specific performance than traditional computer vision methods such as Scale Invariant Feature Transform (SIFT) [31], Generalized Search Tree (GIST)-color [37], Generalized Search Trees (GIST) [36], Histogram of Gradient (HOG) [9], Spatial Pyramid Matching (SPM) [26], etc.

Thus, in this section, we review some of the recent works in chest x-ray classification using DL models [52, 18, 2, 55, 7, 30, 43, 34, 38, 32, 39, 48]. We categorize them into two groups: 2.1 standalone deep learning algorithms and 2.2 ensemble learning algorithms

2.1 Standalone deep learning algorithms

At first, Stephen et al. [52] presented a new model for the detection of pneumonia using DL and machine learning approach. They trained a Convolutional Neural Network (CNN) from scratch using a collection of CXR images. Islam et al [18] devised a Compressed Sensing (CS)-based DL model for the automatic classification of CXR images for pneumonia disease. Similarly, Ayan et al. [2] used DL models on CXR images for early diagnosis of pneumonia. They used Xception [5] and VGG16 [45] pre-trained models. Their results unveil that the VGG16 model outperforms the Xception model in terms of classification accuracy. This strengthens the efficacy of VGG16 model for CXR image representation and classification. Thus, the use of a pre-trained model became widespread in the representation and classification CXR images. For example, Varshni et al. [55] leveraged several pre-trained models such as VGG16 [45], Xception [5], ResNet50 [14], DenseNet121 [17], and DenseNet169 [17] individually as the features extractors and trained four classifiers separately using SVM [15], Random Forest [4], k -nearest neighbors [1], and Naïve Bayes [27] for the classification purpose. Furthermore, Loey et al. [30] used Generative Adversarial Networks (GAN) [12] and fine-tuning on AlexNet [22], ResNet18 [14], and GoogleNet [53] for the classification of the COVID-19 CXR dataset, where images belong to 4 categories. In their method, GAN was used to augment the x-ray images to overcome the over-fitting problem during the training phase. Moreover, Khan et al. [21] devised a new deep learning model using the Xception [5] model, where they performed fine-tuning using CXR images.

Moreover, Ozturk et al. [38] established a new deep learning model for the categorization of COVID-19 related CXR images that uses DarkNet19 [41]. Furthermore, Luz et al. [32] devised another novel deep learning (DL) model, which uses the EfficientNet [54] model, which adopts transfer learning over CXR images for the classification task. Furthermore, Panwar et al. [39] established a new model, which is called nCOVnet, using the VGG16 model, which imparts a prominent accuracy for COVID-19 CXR image analysis. This further claims that the VGG16 model, which was quite popular in the past, is still popular in CXR image analysis. Recently, Sitaula et al. [48] established an attention module on

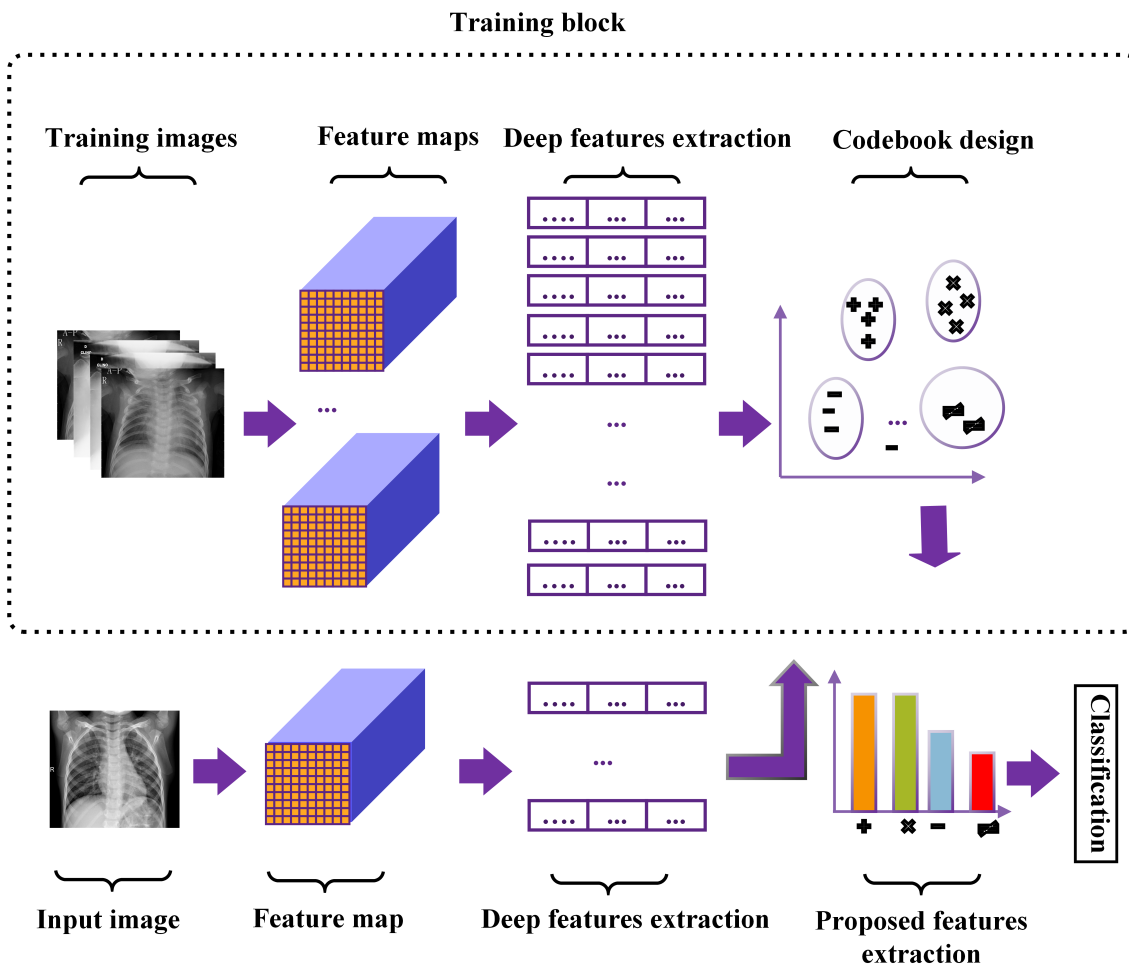


Fig. 2 The overall pipeline of the proposed method. Based on the codebook/dictionary achieved from training block, the proposed features vector is extracted for each input image using the bag of visual features approach.

top of the VGG16 model (AVGG) for the CXR images classification. Their method outperforms several state-of-the-art methods.

2.2 Ensemble learning algorithms

Ensemble learning methods have also been used in CXR image representation and classification where different types of features are combined for better discrimination of images. Zhou et al. [58] proposed an ensemble learning approach of several ANNs for the lung cancer cell identification task. Sasaki et al. [43] established an ensemble learning approach using DL on CXR images. In their method, they performed several filtering and pre-processing operations on images and then ensemble them using DL for the detection of abnormality in CXR images. Li et al. [28] also utilized multiple CNNs to reduce the false positive results on lung nodules of CXR images. Moreover, Islam et al. [18]

designed an ensemble method to aggregate different pre-trained deep learning models for abnormality detection in lung images. Chouhan et al. [7] introduced a model, where the outputs of 5 pre-trained deep learning models, namely AlexNet, ResNet18, DenseNet121, GoogleNet, and Inception-V3, were ensemble for the detection of pneumonia using transfer learning. This helps to learn multiple types of information achieved from various pre-trained DL models to bolster the classification performance. Nevertheless, ensemble learning algorithms are arduous for which we need to be vigilant in hyper-parameter tuning in addition to the overfitting problem.

Most existing methods in the literature need a huge amount of data for fine-tuning DL models and most of them extract high-level features, which may not be sufficient for CXR images. They require mid-level features that are neither more generic nor more specific. In the next section, we introduce our proposed approach to extract such mid-level features.

3 Proposed method

The mid-level features of CXR images can be achieved from the feature maps extracted from the intermediate layers of pre-trained models using a Bag of Visual Words (BoVW) method. Since CXR images are sparse (having few semantic regions), an existing bag of visual words method that has been applied to represent other images (e.g., satellite images) may not work accurately in this domain. To this end, we propose an improved version of a bag of visual words method on deep features to represent CXR images more accurately. In this section, we discuss the steps involved in our proposed feature extraction method. There are three main steps in our method: deep features extraction (Sec. 3.1), unsupervised codebook (dictionary) design (Sec. 3.2), and proposed features extraction (Sec. 3.3). The overall pipeline of the proposed method is shown in Fig. 2.

3.1 Deep features extraction

At first, we extract the deep features from the feature map of the 4th pooling (p_4) layer from VGG16 [45], which is a deep learning model pre-trained on ImageNet [10]. We prefer VGG16 in our work because of three reasons. First, it has a unrivalled performance in recent biomedical image analysis works such as COVID-19 CXR image analysis [48], breast cancer image analysis [47], etc. Second, it is easy to analyze and experiment with its five pooling layers. Third, it uses smaller-sized kernels, which could learn distinguishing features of biomedical images at a smaller level.

We believe that 4th layer of such a model has a higher level of discriminability than other layers as seen in Fig. 3. The detailed discussion about the efficacy of the 4th pooling layer is also presented in Sec. 4.4. Furthermore, we use the VGG16 model due to its simple and prominent features extraction capability in various types of image representation tasks [51, 23, 13]. Authors in [48, 47] highlight the importance of 4th pooling layer compared to other layers in biomedical imaging for separable feature extraction. The size of the features map from the p_4 layer of the VGG16 model is 3-D shape having $H = 14$ (height), $W = 14$ width, and $L = 512$ (length). From each feature map, we achieve 14×14 number of features, each of size 512. Then, each feature vector is L2-normalized. This normalization helps to preserve the separability of deep features of images [13]. Let us say that an input image yields feature map with $14 \times 14 = 196$ number of features vectors that are represented by $x_0, x_1, x_2, \dots, x_{196}$. Each features vec-

tor x_i is of 512-D size (i.e., $|x_i| = 512$), which is then normalized by L2-norm as seen in Eq. (1).

$$x'_i = \frac{x_i}{\|x_i\|_2 + \epsilon} \quad (1)$$

In Eq. (1), the features vector x'_i represents the i^{th} normalized deep features vector extracted from the corresponding feature map. While achieving such features vector, we add $\epsilon = 0.00000008$ with denominator to avoid the divide by zero exception because the feature map obtained for chest x-ray images is sparse and it is more likely to encounter the divide by zero exception in most cases.

3.2 Unsupervised dictionary (codebook) design

We used deep features (extracted from the VGG16 model as discussed above in Sec. 3.1) of all training images to design a dictionary or codebook. Each image provides $\{x'_i\}_{i=1}^{196}$ deep features and let's say there are m training images. Thus, the total number of deep features to design our codebook is $196 \times m$. To design the codebook or dictionary, we utilize a simple, yet popular unsupervised clustering algorithm called k -means [19] that groups deep features having similar patterns into clusters. Given a parameter k , k -means provide k groups or clusters ($\{c_1, c_2, \dots, c_k\}$) of deep features where deep features in each group are similar (i.e., they capture similar patterns of images). We use such k cluster centroids as a dictionary or codebook of deep visual words which is used to extract features for each input image.

3.3 Proposed feature extraction

To extract features of each input image y , we first follow step 3.1 to achieve 196 normalized deep features of y and then, design a histogram based on the dictionary defined in step 3.2. The size of histogram is k (the dictionary size) where each code (cluster centroid) in the dictionary c_j has a weight w_j . All 196 deep features of y are assigned to their nearest centroids. The weight w_j is the number of deep features assigned to the cluster c_j . In other words, histogram is a bag of visual words (centroids) where weights are their frequencies. The resulting features of y is a k -D vector $\{w_1, w_2, \dots, w_k\}$. The extracted bag of visual words features vector is, finally, normalized as in Eq. (1), which acts as our proposed features of the corresponding input image.



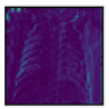
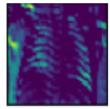
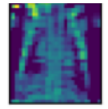
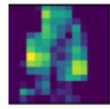



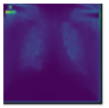
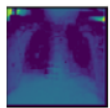
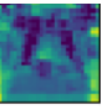
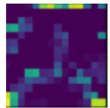



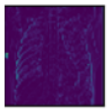
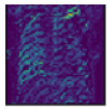
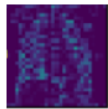
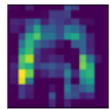



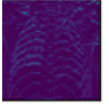
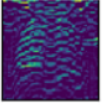
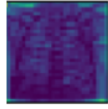
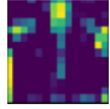

Category	Input image		p_1	p_2	p_3	p_4	p_5
PneumoniaB							
Covid							
Normal							
PneumoniaV							

Fig. 3 Feature maps of an input image from each of the four categories in the COVID-19 dataset extracted from the five pooling layers of VGG16. p_i ($i = 1, 2, \dots, 5$) represents the i^{th} pooling layer.

3.4 Difference between our BoVW and DCF-BoVW features

The main differences between our BoVW and DCF-BoVW features are explained in three different aspects.

Firstly, the L1-normalisation used by the DCF-BoVW method is more suitable for dense images such as satellite images. However, since the chest x-ray images are

sparse in nature, such normalization becomes counter-productive as it masks some discriminating clues. Thus, we eliminate this normalization in our method due to the nature of chest x-ray images.

Secondly, we apply L2-normalisation to the deep features extracted from the unnormalized feature maps to exploit the property of cosine similarity in the k -means clustering. Note that Euclidean distance on the L2-normalised feature is equivalent to using cosine distance. The directions of deep features are more important than their lengths to group vectors with similar patterns into clusters to define our codebook. This will help us to detect sparse patterns in images which can be useful in discriminating abnormalities in x-ray images.

Finally, we replace the L1-normalisation of the final BoVW features used in the DCF-BoVW method by L2-normalisation. Again, this allows us to exploit the property of cosine similarity in the SVM's RBF kernel. Because BoVW features are sparse as many vector entries are zeros, cosine similarity is more appropriate than the Euclidean distance.

4 Experimental setup and comparison

4.1 Dataset

We utilize 4 COVID-19 CXR image datasets that are publicly available. To evaluate our method on such datasets,

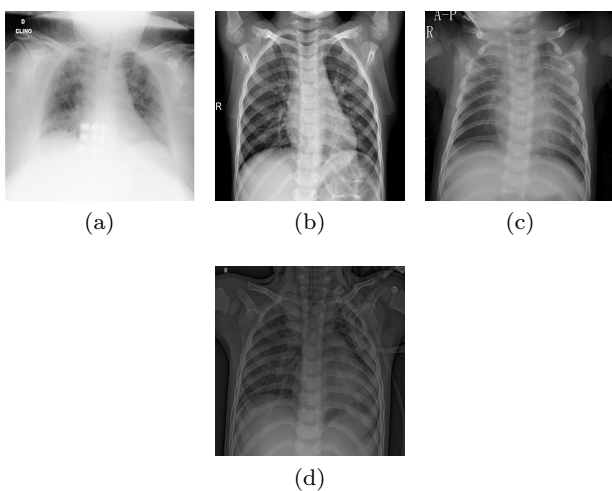


Fig. 4 Example images of chest x-ray images from Dataset 4 [8, 20] for four classes: (a) Covid, (b) Normal, (c) PneumoniaB, and (d) PneumoniaV.

Table 1 Detailed description of datasets used in our work

Dataset	# of images	Categories	Ref.
Dataset 1 (D1)	1,125	Covid-19, Pneumonia, No_findings	[38]
Dataset 2 (D2)	1,638	Covid, Normal, PneumoniaB, PneumoniaV	[21]
Dataset 3 (D3)	2,138	Covid, Normal, No_findings, PneumoniaB, PneumoniaV	[21, 38]
Dataset 4 (D4)	320	Covid, Normal, PneumoniaB, PneumoniaV	[8, 20]

we divide the images of each dataset into a 70:30 ratio for the train:test set for each category. We utilize the average accuracy of five different runs to present in the table for the comparison purpose.

Dataset 1 [38] comprises 3 categories: Covid-19, Pneumonia, and No_findings. Here, each category has at least 125 images. The No_findings category comprises several ambiguous and challenging CXR images.

Dataset 2 [21] comprises 4 categories: Covid, Normal, Pneumonia Viral (PneumoniaV) and Pneumonia Bacteria (PneumoniaB)

Dataset 3 [21, 38] includes 5 categories: Covid, No_findings, Normal, Pneumonia Bacteria (PneumoniaB), and Pneumonia Viral (PneumoniaV). Dataset 3 is the combination of No_finding category from Dataset 1 and other categories from Dataset 2. Here, each category includes at least 320 CXR images.

Dataset 4 [8, 20] has 4 categories: Covid, Normal, PneumoniaV, and PneumoniaB, where each category contains at least 69 images. This dataset has been used by [30], which can be downloaded from the link ³

Example images of covid-19 are shown in Fig. 4. Also, further detailed information of all datasets are provided in Table 1.

4.2 Implementation

To implement our work, we use Keras [6] implemented in Python [42]. Keras is used to implement the pre-trained model in our work. We use the number of clusters $k = 400$ in k -means clustering to define the dictionary to extract proposed features. For the classification purpose, we use a Support Vector Machine (SVM) classifier implemented using Scikit-learn [40] in Python. We normalize and standardize our features to feed into

³ COVID-19 Dataset Available online: <https://drive.google.com/uc?id=1coM7x3378f-Ou2l6Pg2w1daOI7Dntu1a> (accessed on Apr 17, 2020).

Table 2 Comparison with previous methods on four datasets (D1, D2, D3, and D4) using average classification accuracy (%) over five runs. Note that - represents the unavailable accuracy because of the over-fitting problems in existing DL-based methods using transfer learning on D4.

Method	D1 (%)	D2 (%)	D3 (%)	D4 (%)
DCF-BoVW, 2018 [56]	75.31	81.53	83.72	72.46
CoroNet, 2020 [21]	76.82	80.60	83.41	-
Luz et al., 2020 [32]	47.51	84.29	79.96	-
nCOVnet, 2020 [39]	62.95	70.62	67.67	-
AVGG, 2020 [48]	79.58	85.43	87.49	-
Ours	82.00	87.86	87.92	83.22

the SVM classifier. Moreover, we fix the kernel as radial basis function (*RBF*) and γ parameter as $1e - 05$ in SVM. We automatically tune the cost parameter C in the range of $\{1, 10, 20, \dots, 100\}$ on the training set using a 5-fold cross-validation method and use the optimal setting to train the model using the entire training set and test on the test set. We execute all our experiments on a workstation with NVIDIA Geforce GTX 1050 GPU and 4 GB RAM.

4.3 Comparison with state-of-the-art methods

We present the results of the experiments conducted to compare our method with five recent state-of-the-art methods (one method uses the BoW approach over deep features and four methods adopt transfer-learning approach) that are based on pre-trained models on four CXR image datasets (D1, D2, D3, and D4) in Table 2. In the table, the second, third, fourth, and fifth columns enlist the accuracies of contending methods in D1, D2, D3, and D4, respectively. Note that the accuracies reported in the table are averaged accuracy of five runs for each method.

Results in the second column of Table 2 show that our method outperforms all five contenders with the accuracy of 82.00% on D1. This further highlights that it imparts the performance increment of at least 2.50% from the second-best method (AVGG [48]) and at least 40% accuracy from the worst method (Luz et al. [32]). Similarly, on D2 in the third column of Table 2, we notice that our method outperforms all five methods with an accuracy of 87.86%, which is at least 2.43% higher than the second-best method (AVGG [48]) and at least 17% higher than the worst-performing method (nCOVnet [39]). In the fourth column of Table 2 on D3, we ob-

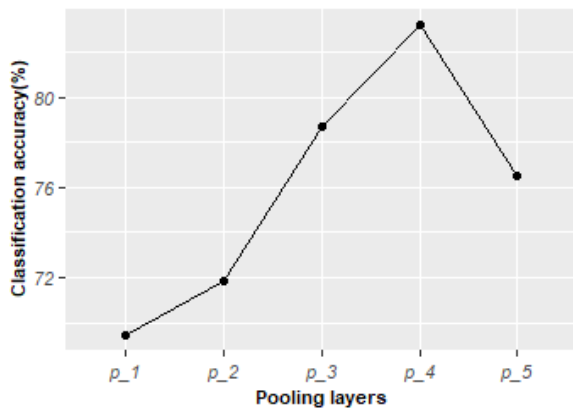


Fig. 5 Average classification accuracy (%) achieved by our method on D4 using deep features extracted from the five pooling layers (p_1 to p_5) of the VGG16 model.

serve that our method, which yields 87.92% accuracy, is superior to the second-best method (AVGG [48]) with a slim margin of 0.43%, whereas it imparts over 20% accuracy against the worst performing method (nCOV-net [39]). Last but not the least, in the fifth column of Table 2 on D4, we notice that our method, which produces 83.22%, outperforms the DCF-BoVW [56] with the margin of over 10% accuracy. Please note that for D4, we only compare our method with DCF-BoVW [56], which can work for a limited amount of data, only and do not compare with other DL-based methods that uses transfer learning because this dataset has a very limited number of CXR images.

The comparison of our method against five different recent DL-based methods on four datasets unveils that our method provides a stable and prominent performance. This result further underscores that the classification performance of the bag of words approach, which capture the more detailed spatial information of deteriorated regions more accurately than other methods, seems more appropriate to CXR image analysis (e.g., COVID-19 CXR images) than other DL-based methods using transfer learning approach.

4.4 Ablative study of pooling layers

In this subsection, we present the results of an ablative study on D4, which is the smallest dataset, to analyze the effect on the classification accuracy of using deep features from the five different pooling layers of VGG16 in our method. The detailed results are presented in Fig. 5. While observing the line graph, we notice that the 4th pooling layer of the VGG16 model produces highly separable features than other pooling layers on the COVID-19 dataset.

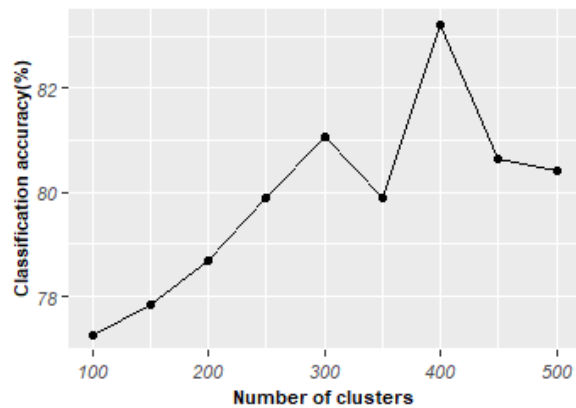


Fig. 6 Average classification accuracy (%) with different cluster number on D4. Note that deep features from the 4th pooling layer (p_4) were used.

4.5 Ablative study of cluster numbers

We analyze different number of unsupervised patterns to be used in our experiments on D4. For this, we vary the cluster numbers from 100 to 500 using the interval of 50 and present the results in Fig. 6. From the line graph, we notice that the appropriate number of clusters that produce the best result is $k = 400$.

4.6 Ablative study of class-wise performance

We study the average class-wise performance of our method on D4. The average class-wise performance are reported using precision, recall, and f1-score, which are defined in Eqs. (2),(3), and (4), respectively.

$$\text{Precision} = \frac{TP}{TP + FP}, \quad (2)$$

$$\text{Recall} = \frac{TP}{TP + FN}, \quad (3)$$

$$\text{F1-score} = \frac{2 \times (\text{Recall} \times \text{Precision})}{(\text{Recall} + \text{Precision})}, \quad (4)$$

where TP , FP , and FN represent true positive, false positive, and false negative results, respectively. We present the average precision, recall, and f1-score in Table 3. The results show the discriminability of our proposed method in all four classes. It shows that our method can distinguish the Covid and normal class well and there is some confusion among two pneumonia classes.

Table 3 Average class-wise study (%) over five runs of our method on D4 using precision, recall, and f1-score.

Class	Precision (%)	Recall (%)	F1-score (%)
Covid	100.00	97.20	98.40
Normal	94.20	93.60	93.80
PneumoniaB	75.80	67.60	71.00
PneumoniaV	68.00	76.80	71.80

5 Conclusion and future works

In this paper, we propose a new feature extraction method based on Bag of Deep Visual Words (BoDVW) to represent chest x-ray images. Empirical results on the classification of chest x-ray images using the COVID-19 dataset show that our method is more appropriate to represent chest x-ray images. This is mainly because our features can capture a few interesting regions (sparse markers) indicating abnormalities well. Our features are extracted using a visual dictionary defined by the clustering of deep features from all training images. Therefore, they can capture patterns in each training image and thus helps to capture potential markers for various lung infections such as COVID-19 and pneumonia. Also, the size of our proposed features is relatively very small compared to other existing methods and our method runs faster than other existing methods.

Though the evaluation is done on a relatively small dataset, our method shows promising results to detect and distinguish lung infection due to pneumonia and COVID-19. COVID-19 being a relatively new disease and there are not a lot of chest x-ray images available. Nevertheless, given the current crisis with the COVID-19 pandemic, our method which is accurate and fast can be very useful for health professionals for mass screening of people for COVID-19. Accurate detection and distinction of lung infections due to COVID-19 and pneumonia are very important for COVID-19 diagnosis as people infected by these diseases show similar symptoms.

In the future, it would be interesting to verify our results in a large study with more sample images including other types of lung infection such as tuberculosis. Another potential direction is to investigate if a similar approach can be used to represent other types of medical images such as CT scans, histopathological images, colonoscopy images, etc.

References

- Altman NS (1992) An introduction to kernel and nearest-neighbor nonparametric regression. *The American Statistician* 46(3):175–185

- Ayan E, Ünver HM (2019) Diagnosis of pneumonia from chest x-ray images using deep learning. In: *In Proc. Scientific Meeting on Electrical-Electronics & Biomedical Engineering and Computer Science (EBBT)*, pp 1–5
- Bastola A, Sah R, Rodriguez-Morales AJ, Lal BK, Jha R, Ojha HC, Shrestha B, Chu DK, Poon LL, Costello A, et al. (2020) The first 2019 novel coronavirus case in nepal. *The Lancet Infectious Diseases* 20(3):279–280
- Breiman L (2001) Random forests. *Machine learning* 45(1):5–32
- Chollet F (2017) Xception: Deep learning with depthwise separable convolutions. In: *Proc. IEEE Conf. Comput. Vis. Pattern Recognit.*, pp 1251–1258
- Chollet F, et al. (2015) Keras. <https://github.com/fchollet/keras>
- Chouhan V, Singh SK, Khamparia A, Gupta D, Tiwari P, Moreira C, Damaševičius R, de Albuquerque VHC (2020) A novel transfer learning based approach for pneumonia detection in chest x-ray images. *Applied Sciences* 10(2):559
- Cohen JP, Morrison P, Dao L (2020) Covid-19 image data collection. *arXiv preprint arXiv:200311597*
- Dalal N, Triggs B (2005) Histograms of oriented gradients for human detection. In: *Proc. IEEE Comput. Soc. Conf. Comput. Vis. Pattern Recognit. (CVPR)*, pp 886–893
- Deng J, Dong W, Socher R, Li LJ, Li K, Fei-Fei L (2009) ImageNet: a large-scale hierarchical image database. In: *Proc. IEEE Conf. Comput. Vis. Pattern Recognit. (CVPR)*
- Giovanetti M, Benvenuto D, Angeletti S, Ciccozzi M (2020) The first two cases of 2019-ncov in italy: Where they come from? *Journal of medical virology*
- Goodfellow I, Pouget-Abadie J, Mirza M, Xu B, Warde-Farley D, Ozair S, Courville A, Bengio Y (2014) Generative adversarial nets. In: *Proc. Advances in Neural Information Processing Systems*, pp 2672–2680
- Guo Y, Liu Y, Lao S, Bakker EM, Bai L, Lew MS (2018) Bag of surrogate parts feature for visual recognition. *IEEE Trans Multimedia* 20(6):1525–1536
- He K, Zhang X, Ren S, Sun J (2016) Deep residual learning for image recognition. In: *Proc. IEEE Conf. on Computer Vision and Pattern Recognition (CVPR)*, pp 770–778
- Hearst MA (1998) Support vector machines. *IEEE Intelligent Systems* 13(4):18–28

16. Holshue ML, DeBolt C, Lindquist S, Lofy KH, Wiesman J, Bruce H, Spitters C, Ericson K, Wilkerson S, Tural A, et al. (2020) First case of 2019 novel coronavirus in the united states. *New England Journal of Medicine*
17. Huang G, Liu Z, Van Der Maaten L, Weinberger KQ (2017) Densely connected convolutional networks. In: *Proc. IEEE Conf. Comput. Vis. Pattern Recognit.*, pp 4700–4708
18. Islam SR, Maity SP, Ray AK, Mandal M (2019) Automatic detection of pneumonia on compressed sensing images using deep learning. In: *In Proc. Canadian Conference of Electrical and Computer Engineering (CCECE)*, pp 1–4
19. Jin X, Han J (2010) *K-Means Clustering*, Springer US, Boston, MA, pp 563–564
20. Kermany DS, Goldbaum M, Cai W, Valentim CC, Liang H, Baxter SL, McKeown A, Yang G, Wu X, Yan F, et al. (2018) Identifying medical diagnoses and treatable diseases by image-based deep learning. *Cell* 172(5):1122–1131
21. Khan A, Shah J, Bhat M (2020) Coronet: A deep neural network for detection and diagnosis of covid-19 from chest x-ray images. *Computer Methods and Programs in Biomedicine* 196:105581
22. Krizhevsky A, Sutskever I, Hinton GE (2012) Imagenet classification with deep convolutional neural networks. In: *Proc. Adv. Neural Inf. Process. Syst. (NIPS)*, pp 1097–1105
23. Kumar A, Singh SK, Saxena S, Lakshmanan K, Sangaiah AK, Chauhan H, Shrivastava S, Singh RK (2020) Deep feature learning for histopathological image classification of canine mammary tumors and human breast cancer. *Information Sciences* 508:405–421
24. Lai CC, Shih TP, Ko WC, Tang HJ, Hsueh PR (2020) Severe acute respiratory syndrome coronavirus 2 (sars-cov-2) and corona virus disease-2019 (covid-19): the epidemic and the challenges. *International Journal of Antimicrobial Agents* p 105924
25. Latinne A, Hu B, Olival KJ, Zhu G, Zhang L, Li H, Chmura AA, Field HE, Zambrana-Torrel C, Epstein JH, Li B, Zhang W, Wang LF, Shi ZL, Daszak P (2020) Origin and cross-species transmission of bat coronaviruses in china. *Nature Communications* 11(4235), DOI 10.1038/s41467-020-17687-3
26. Lazebnik S, Schmid C, Ponce J (2006) Beyond bags of features: Spatial pyramid matching for recognizing natural scene categories. In: *Proc. IEEE Comput. Soc. Conf. Comput. Vis. Pattern Recognit.*, pp 2169–2178
27. Lewis DD (1998) Naive (bayes) at forty: The independence assumption in information retrieval. In: *Proc. European Conference on Machine Learning*, pp 4–15
28. Li C, Zhu G, Wu X, Wang Y (2018) False-positive reduction on lung nodules detection in chest radiographs by ensemble of convolutional neural networks. *IEEE Access* 6:16060–16067
29. Li J, Li JJ, Xie X, Cai X, Huang J, Tian X, Zhu H (2020) Game consumption and the 2019 novel coronavirus. *The Lancet Infectious Diseases* 20(3):275–276
30. Loey M, Smarandache F, M Khalifa NE (2020) Within the lack of chest covid-19 x-ray dataset: a novel detection model based on gan and deep transfer learning. *Symmetry* 12(4):651
31. Lowe DG (2004) Distinctive image features from scale-invariant keypoints. *International Journal of Computer Vision* 60(2):91–110
32. Luz E, Silva PL, Silva R, Moreira G (2020) Towards an efficient deep learning model for covid-19 patterns detection in x-ray images. *arXiv preprint arXiv:200405717*
33. Maaten L, Hinton G (2008) Visualizing data using t-sne. *Journal of machine learning research* 9(Nov):2579–2605
34. Narin A, Kaya C, Pamuk Z (2020) Automatic detection of coronavirus disease (covid-19) using x-ray images and deep convolutional neural networks. *arXiv preprint arXiv:200310849*
35. Nguyen TT, Abdelrazek M, Nguyen DT, Aryal S, Nguyen DT, Khatami A (2020) Origin of novel coronavirus (covid-19): A computational biology study using artificial intelligence. *bioRxiv* DOI 10.1101/2020.05.12.091397
36. Oliva A (2005) Gist of the scene. In: *Neurobiology of Attention*, pp 251–256
37. Oliva A, Torralba A (2001) Modeling the shape of the scene: a holistic representation of the spatial envelope. *Int J Comput Vis* 42(3):145–175
38. Ozturk T, Talo M, Yildirim EA, Baloglu UB, Yildirim O, Acharya UR (2020) Automated detection of covid-19 cases using deep neural networks with x-ray images. *Computers in Biology and Medicine* p 103792
39. Panwar H, Gupta P, Siddiqui MK, Morales-Menendez R, Singh V (2020) Application of deep learning for fast detection of covid-19 in x-rays using ncovnet. *Chaos, Solitons & Fractals* p 109944
40. Pedregosa F, Varoquaux G, Gramfort A, Michel V, Thirion B, Grisel O, Blondel M, Prettenhofer P, Weiss R, Dubourg V, et al. (2011) Scikit-learn: Machine learning in python. *Journal of Machine Learning Research* 12:2825–2830

41. Redmon J, Farhadi A (2017) Yolo9000: better, faster, stronger. In: Proc. IEEE Conf. Comput. Vis. Pattern Recognit. (CVPR), pp 7263–7271
42. Rossum G (1995) Python reference manual. Tech. rep., Amsterdam, The Netherlands
43. Sasaki T, Kinoshita K, Kishida S, Hirata Y, Yamada S (2012) Ensemble learning in systems of neural networks for detection of abnormal shadows from x-ray images of lungs. *Journal of Signal Processing* 16(4):343–346
44. Sharfstein JM, Becker SJ, Mello MM (2020) Diagnostic testing for the novel coronavirus. *Jama*
45. Simonyan K, Zisserman A (2014) Very deep convolutional networks for large-scale image recognition. arXiv preprint arXiv:14091556
46. Singhal T (2020) A review of coronavirus disease-2019 (covid-19). *The Indian Journal of Pediatrics* pp 1–6
47. Sitaula C, Aryal S (2020) Fusion of whole and part features for the classification of histopathological image of breast tissue. *Health Information Science and Systems* 8(1):1–12
48. Sitaula C, Hossain M (2020) Attention-based vgg-16 model for covid-19 chest x-ray image classification. *Applied Intelligence* pp 1–14
49. Sitaula C, Aryal S, Xiang Y, Basnet A, Lu X (2020) Content and context features for scene image representation. arXiv preprint arXiv:200603217
50. Sitaula C, Xiang Y, Aryal S, Lu X (2020) Scene image representation by foreground, background and hybrid features. arXiv preprint arXiv:200603199
51. Sitaula C, Xiang Y, Basnet A, Aryal S, Lu X (2020) Hdf: hybrid deep features for scene image representation. In: Proc. International Joint Conference on Neural Networks (IJCNN), pp 1–8
52. Stephen O, Sain M, Maduh UJ, Jeong DU (2019) An efficient deep learning approach to pneumonia classification in healthcare. *Journal of healthcare engineering* 2019
53. Szegedy C, Liu W, Jia Y, Sermanet P, Reed S, Anguelov D, Erhan D, Vanhoucke V, Rabinovich A (2015) Going deeper with convolutions. In: Proc. IEEE Conf. Comput. Vis. Pattern Recognit. (CVPR), pp 1–9
54. Tan M, Le QV (2019) Efficientnet: Rethinking model scaling for convolutional neural networks. arXiv preprint arXiv:190511946
55. Varshni D, Thakral K, Agarwal L, Nijhawan R, Mittal A (2019) Pneumonia detection using cnn based feature extraction. In: In Proc. International Conference on Electrical, Computer and Communication Technologies (ICECCT), pp 1–7
56. Wan J, Yilmaz A, Yan L (2018) Dcf-bow: Build match graph using bag of deep convolutional features for structure from motion. *IEEE Geoscience and Remote Sensing Letters* 15(12):1847–1851
57. Zhou B, Khosla A, Lapedriza A, Torralba A, Oliva A (2016) Places: An image database for deep scene understanding. arXiv preprint arXiv:161002055
58. Zhou ZH, Jiang Y, Yang YB, Chen SF (2002) Lung cancer cell identification based on artificial neural network ensembles. *Artificial Intelligence in Medicine* 24(1):25–36